Skin Membrane Electrical Impedance Properties under the Influence of a Varying Water Gradient

Sebastian Björklund,[†‡*] Tautgirdas Ruzgas,[‡*] Agnieszka Nowacka,[†] Ihab Dahi,[‡] Daniel Topgaard,[†] Emma Sparr,[†] and Johan Engblom[‡]

[†]Division of Physical Chemistry, The Center for Chemistry and Chemical Engineering, Lund University, Lund, Sweden; and [‡]Biomedical Laboratory Science and Technology, Faculty of Health and Society, Malmö University, Malmö, Sweden

ABSTRACT The stratum corneum (SC) is an effective permeability barrier. One strategy to increase drug delivery across skin is to increase the hydration. A detailed description of how hydration affects skin permeability requires characterization of both macroscopic and molecular properties and how they respond to hydration. We explore this issue by performing impedance experiments on excised skin membranes in the frequency range 1 Hz to 0.2 MHz under the influence of a varying gradient in water activity (a_w). Hydration/dehydration induces reversible changes of membrane resistance and effective capacitance. On average, the membrane resistance is 14 times lower and the effective capacitance is 1.5 times higher when the outermost SC membrane is exposed to hydrating conditions ($a_w = 0.992$), as compared to the case of more dehydrating conditions ($a_w = 0.826$). Molecular insight into the hydration effects on the SC components is provided by natural-abundance ^{13}C polarization transfer solid-state NMR and x-ray diffraction under similar hydration conditions. Hydration has a significant effect on the dynamics of the keratin filament terminals and increases the interchain spacing of the filaments. The SC lipids are organized into lamellar structures with ~ 12.6 nm spacing and hexagonal hydrocarbon chain packing with mainly all-*trans* configuration of the acyl chains, irrespective of hydration state. Subtle changes in the dynamics of the lipids due to mobilization and incorporation of cholesterol and long-chain lipid species into the fluid lipid fraction is suggested to occur upon hydration, which can explain the changes of the impedance response. The results presented here provide information that is useful in explaining the effect of hydration on skin permeability.

INTRODUCTION

Skin has many functions that are important for body homeostasis. One major function is to serve as a transport barrier against molecular diffusion. The skin barrier effectively restricts both inward and outward diffusion of most molecules and thus upholds the water balance and protects us from harmful substances entering the body (1). Drug delivery through the skin is attractive for drug therapy, since skin is easily accessible and this route avoids first-pass metabolism. For transdermal delivery, where one wants the drug to reach the systemic circulation, the transport barrier of skin has to be overcome to obtain effective uptake. Common strategies that can increase the systemic distribution of transdermal drugs are to increase skin hydration (e.g., by occluding the skin) (2,3) or to introduce so-called chemical penetration enhancers (4). Physical forces such as electrical voltage, e.g., iontophoresis and electroporation, can also be used to overcome the skin barrier (5). Iontophoresis is a method by which charged or neutral molecules are transported from an electrolyte solution into and/or through the skin by application of a small electrical current, whereas electroporation increases skin permeability by applying short high-voltage pulses that are suggested to induce structural perturbation of the stratum corneum (SC), allowing for increased drug transport (6). It is clear that exploration of these methods relies on good characterization of the electrical impedance properties of the skin membrane, which also helps in evaluation of mechanisms of drug transport across skin (7,8). A thorough description of the skin membrane resistance and capacitance properties is also relevant for commercially available equipment for assessing skin hydration (e.g., SKICON, Corneometer, etc.), which rely on conductance or capacitance measurements of the skin barrier (9).

The barrier function is assured by the outermost skin layer, the SC. The SC is only a few micrometers thick and contains a continuous extracellular matrix of lipid lamellae that surrounds the keratinized cells (corneocytes) in a three-dimensional manner (10). The SC lipids comprise a heterogeneous mixture of mainly free fatty acids, cholesterol, and ceramides (11). The intracellular space of the corneocytes is filled predominantly with keratin filaments, which are enclosed by a cornified envelope of cross-linked proteins and covalently bound lipids (12–14). The electrical properties of skin have been widely studied both in vivo and in vitro, and it is established that the impedance of skin resides foremost within the SC, whereas the impedance of the underlying viable layers is orders of magnitude lower (15–17). A common model of skin impedance characteristics is an equivalent circuit consisting of a leading resistor in series with a parallel arrangement of a resistor and a capacitor (7,15). The leading resistor (R_{sol}) models the resistance from the electrolyte and the underlying viable tissue, whereas the parallel resistor (R_{mem}) is associated with ion-conductive pathways in the SC, which may include the

Submitted February 5, 2013, and accepted for publication May 2, 2013.

*Correspondence: Sebastian.Bjorklund@fkem1.lu.se or Tautgirdas.Ruzgas@mah.se

Editor: Klaus Gawrisch.

0006-3495/13/06/2639/12 $2.00

http://dx.doi.org/10.1016/j.bpj.2013.05.008

extracellular and intracellular routes, as well as through the appendages. The capacitor (C) has been associated with restriction of ion transfer at low conductive lipid and lipid-protein domains of the SC (8,16,18,19). In the case of in vitro studies on excised skin membranes, representative values of these elements are on the order of $R_{sol} \sim 200$ Ohm cm^2, $R_{mem} \sim 10$–200 kOhm cm^2, and $C \sim 10$–50 nF cm^{-2} (7,8,20).

Numerous studies have shown that the SC behaves as a responding membrane in that its biophysical properties can be regulated by external parameters, such as relative humidity (RH) (2,17,21–23). The water gradient across skin regulates the degree of SC hydration, and we showed previously that changes in the water gradient can be used to regulate molecular transport through the skin in a reversible manner (2). In those experiments, the gradient in water activity across the skin membrane was strictly controlled and defined by the water activities in the surrounding solutions. In this study, we explore how changes in the water gradient across the skin membrane affect its electrical impedance properties by employing similar experimental conditions. Here, the water activity on the SC side of the skin membrane varies between $a_w = 0.826$ and $a_w = 0.992$, whereas the water activity on the dermal side is kept at physiological conditions ($a_w = 0.992$). We measure the impedance of skin membranes under the influence of a varying water gradient, and from these measurements we obtain clear trends in the responding changes in skin membrane resistance and effective capacitance. We provide molecular insight into the hydration effects on the SC membrane from natural-abundance ^{13}C polarization-transfer solid-state NMR methods (PT ssNMR) (24) and small- and wide-angle x-ray diffraction (SAXD and WAXD, respectively) measurements. We confirm that hydration has a strong effect on the skin membrane resistance (17,21,23) and show that these changes are reversible. We show that hydration increases the skin membrane capacitance, an effect that is also shown to be reversible. The observed effects are attributed to hydration-induced alterations of the SC molecular dynamics, as shown from PT ssNMR experiments, and subtle alterations of the molecular organization, as observed by SAXD and WAXD measurements.

MATERIALS AND METHODS

Materials

Ultragrade poly(ethylene glycol) 1500 Da (PEG) was obtained from Sigma-Aldrich (St. Louis, MO). NaCl, $Na_2HPO_4 \bullet 2H_2O$, KH_2PO_4, KNO_3, and K_2SO_4 were purchased from Merck (Whitehouse Station, NJ). Phosphate-buffered saline (PBS) (130.9 mM NaCl, 5.1 mM $Na_2HPO_4 \bullet 2H_2O$, and 1.5 mM KH_2PO_4, pH 7.4) was prepared from Milli-Q water.

Preparation of skin membranes and SC samples

Pig ears were obtained from a local abattoir (Dalsjöfors Slakteri, Borås, Sweden) and stored at −80°C until use. Split-thickness skin membranes from the inside of the outer ear were prepared with a dermatome (TCM 3000 BL, Nouvag, Konstanz, Germany) and punched out to fit the Franz cell used for impedance measurements. The thickness of the skin membranes was ~ 500 μm and the diameter was 1.6 cm. SC samples were prepared from dermatomed skin strips placed on filter paper soaked in 0.2% trypsin in PBS solution for 12 h at 4°C. The SC was removed with forceps and washed thoroughly with cotton-tipped applicators in PBS solution to remove underlying tissue; it was then stored dry in a freezer until use. The SC was equilibrated in PBS solution, $a_w = 0.992$ (25), or in 65 wt % PEG in PBS solution, $a_w = 0.826$ (2), for 24 h at 32°C. Next, the SC was removed from the formulation and gently wiped with paper tissues to remove excess formulation and transferred to either a solid-state NMR or an x-ray diffraction sample cell for measurement. For comparison, pulverized SC samples were equilibrated at corresponding relative humidity (RH) at 32°C for 48 h. NaCl solutions (5.12 and 0.156 mol kg^{-1}) were used to control the RH in two desiccators at 80% RH or 99.5% RH, respectively (26). Control experiments are presented in Figs. S4 and S5 in the Supporting Material.

Impedance spectroscopy measurements of skin membranes under the influence of a varying water gradient

Electrical impedance measurements were conducted at 32°C with a Franz cell equipped with four electrodes and connected to a potentiostat from Ivium Technologies (Eindhoven, The Netherlands), as shown in Fig. S1 *A*. The frequency range was from 1 Hz to 0.2 MHz with five frequencies per decade. The amplitude of the applied voltage was in the range 50–100 mV, ensuring low current densities in the lower frequency range. The experiments were designed taking into consideration the natural variability in skin membrane impedance, reported previously (7,20,23,27,28). Our experimental design circumvents this natural site variability, as it generates experimental data from the same membrane with the water gradient as the varying parameter. The skin membrane was mounted in the Franz cell filled with degassed PBS receptor solution. To allow the skin membrane to be adjusted in terms of temperature and hydration we waited 1 h before the donor chamber was filled with 1 ml of 65 wt % PEG in PBS solution. After 24 h the PEG solution was exchanged for 1 ml neat PBS solution. This cycle was then repeated (i.e., four consecutive 24-h periods and 96 h total). The water gradient across the skin membrane is defined by the boundary conditions of the receptor and donor solutions on either side of the skin membrane. We express the water gradient in terms of the water activity, a_w, defined as the ratio of the vapor pressure above a solution and the vapor pressure above pure water at a specific temperature and pressure ($a_w = p/p_0$). The water activity of 65 wt % PEG in PBS solution is $a_w = 0.826$ (2) and the water activity of the PBS solution is $a_w = 0.992$ (25). We stress the importance of recognizing that the size of PEG (i.e., 1500 Da) assures that the polymer does not penetrate the SC (29,30) and only acts as a dehydrating agent. Several impedance measurements were recorded during the first and last hours of each 24-h period. Between longer periods of impedance measurements, the reference and sensing electrodes were removed to avoid KCl leakage, and the chamber was covered with parafilm to avoid evaporation of water.

PT ssNMR measurements

The NMR technique used, PT ssNMR (24), provides ^{13}C spectra with sufficient resolution to differentiate molecular segments and gives qualitative information on the dynamics of the resolved molecular segments (24,31). In brief, PT ssNMR includes three separate ^{13}C NMR experiments: direct polarization (DP), refocused insensitive nuclei enhanced by protein transfer (INEPT) (32), and ramped cross-polarization (CP) (33). In general, all ^{13}C nuclei are visible in the DP spectrum, whereas the peak intensity in

the INEPT and CP spectra depends on the dynamics of the ^{13}C nuclei: the INEPT spectrum shows mobile molecular segments and the CP spectrum shows rigid molecular segments. In particular, the relation between the INEPT and CP signal intensities depends on the motional anisotropy and the rate of reorientation of the ^{1}H-^{13}C bonds, which can be quantified by the order parameter $|S_{CH}|$ and the motional correlation time, τ_c, respectively (24,31). As demonstrated in Fig. 1, the range of τ_c can be divided into four dynamic regimes, which give rise to characteristic relative intensities in the PT ssNMR experiment (31). The CP signal intensity is maximized in the slow regime, whereas the amplitude from INEPT is zero. In the intermediate regime the signal from both CP and INEPT is zero. In the fast-intermediate regime, CP gives signal, whereas no signal is obtained from INEPT. Finally, in the fast regime, the CP and INEPT signal intensities are independent of τ_c, but are dependent on the motional anisotropy given by $|S_{CH}|$. For anisotropic reorientation, $|S_{CH}| > 0.5$, the CP signal is maximized, whereas the INEPT amplitude is zero. For nearly isotropic motion, $|S_{CH}| < 0.01$, this relation is reversed, with maximized INEPT amplitude and zero CP signal. Equal signals from CP and INEPT are achieved when $|S_{CH}| \approx 0.1$.

After equilibration, the SC was placed in watertight sample containers and transferred to 4-mm rotors (Bruker, Karlsruhe, Germany). NMR experiments were performed on a Bruker Avance-II 500 spectrometer, equipped with a 4-mm CP/magic-angle spinning (MAS) HX probe, at ^{1}H and ^{13}C resonance frequencies of 500 and 125 MHz, respectively. ^{13}C spectra were acquired at a magnetic field of 11.74 T under 68 kHz two-pulse phase-modulated ^{1}H decoupling (34), with 2048 scans/experiment and a recycle delay of 5 s, using a spectral width of 250 ppm and an acquisition time of 50 ms. The spinning frequency was set to $\omega_R/2\pi = 5$ kHz. The ^{13}C spectra were externally referenced to the methylene signal of solid α-glycine at 43.7 ppm. ^{1}H and ^{13}C hard pulses were applied at $\omega_1^{H/C}/2\pi = 80$ kHz. Ramped CP was performed with the contact time 1 ms, the ^{13}C nutation frequency 80 kHz and the ^{1}H nutation frequency linearly ramped from 72 to 88 kHz. The delays $\tau = 1.8$ ms and $\tau' = 1.2$ ms were used in INEPT. The temperature was 32°C, taking into account sample heating induced by MAS and radiofrequency pulses. The experimental time-domain data were processed with line broadening of 30 Hz, zero-filling from 1597 to 8192 time-domain points, Fourier transform, automatic phase correction (35), and baseline correction in Matlab (www.mathworks.com) using in-house code partially derived from matNMR (36).

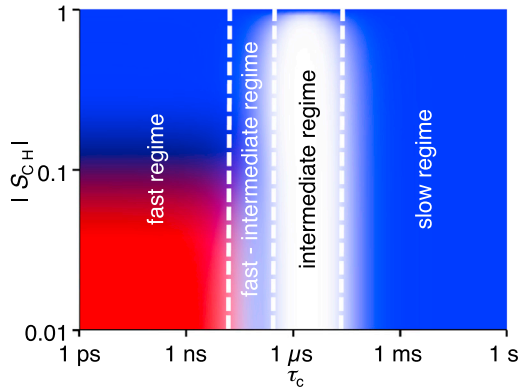

FIGURE 1 Dynamic regimes of the PT ssNMR experiments. Theoretical ^{1}H-to-^{13}C polarization transfer efficiency for a CH_2 segment at 11.74 T magnetic field and 5 kHz MAS as a function of correlation time, τ_c, and order parameter, $|S_{CH}|$. The input parameters for the calculated intensities are equal to the experimental settings. Color codes are given according to the calculated intensities of the INEPT (red) and CP (blue) polarization transfer schemes. A total absence of signal for both INEPT and CP is represented by white. Adapted from Nowacka et al. (31).

Small- and wide-angle x-ray scattering measurements

After equilibration, the SC was folded several times and loaded into the sample holder. The measurements were performed at Maxlab (Lund, Sweden) at the Swedish-Danish beamline Cassiopeia (I911-4, $\lambda = 0.91$ Å) (37). Data collection was performed for a period of 100 s for each sample at 32°C. The intensity was corrected for air scattering (empty cell) and primary-beam intensity changes and plotted as a function of the scattering vector Q, defined as $Q = (4\pi \sin\theta)/\lambda$, where θ and λ are the scattering angle and the wavelength, respectively.

Analysis of impedance data

Impedance data of skin are often modeled with a resistor in series with a parallel combination of a resistor and a capacitor (7,15). This model with ideal (linear) elements is attractive due to its simplicity in terms of data analysis and the fact that the elements can be physically connected to different SC components in a justified manner, as described in the Introduction. However, most biological systems, including skin, are associated with nonlinear properties (38), and this model therefore fails to represent the experimental impedance properties accurately. Several circuits of varying complexity have been proposed to more closely model the electrical properties of skin (18,39,40). Taken together, there is no equivalent circuit that unambiguously describes the impedance properties of skin. In this work, we employed a frequently used circuit for skin impedance data, consisting of a resistor (solution resistance (R_{sol})) in series with a parallel arrangement of a resistor (skin membrane resistance (R_{mem})) and a constant-phase element (CPE) (19,41–43). The CPE is an empirical element that accounts for the nonlinear distribution of time constants and can be used to derive an effective capacitance of the skin membrane (44). The circuit is presented in Fig. S1 *B*, and the method used for analyzing the impedance data is presented in the following text in terms of the equivalent circuit components. Other equivalent circuits were considered and used for analysis, without providing further understanding or changing our conclusions; see Supporting Material, Text A.

Membrane resistance (R_{mem}) and solution resistance (R_{sol})

All impedance data on skin membranes displayed the same characteristic pattern of a depressed semicircle when presented as impedance plane plots (see Supporting Material, Text B, for more details). R_{sol} and R_{mem} were determined by fitting the data in impedance plane plots to the equivalent circuit using Ivium software. All data were normalized with the skin membrane area (0.64 cm^2) to get units in Ohm cm^2.

Effective membrane capacitance, C_{eff}

The total impedance, Z, of the equivalent circuit is given by Eq. 1.

$$Z = R_{sol} + \frac{R_{mem}}{1 + (i2\pi f)^{\alpha} Q R_{mem}} \quad (1)$$

Here, $2\pi f$ is the angular frequency, and Q and α are CPE parameters. When α equals unity, Q represents an ideal capacitor with units of F m^{-2}. In this work, α was on the order of ~ 0.70–0.85, consistent with several impedance studies on skin (19,40,41). The CPE parameters account for the depression of the semicircle and can be used to estimate the effective capacitance of the skin membrane when the time constants describing the impedance response follow a normal distribution across the skin (41). In this case, an effective CPE coefficient, Q_{eff}, can be derived

from the high-frequency region where Q_{eff} in theory provides a correct value of Q in the case when α equals unity (44). The CPE parameters α and Q_{eff} were obtained from the imaginary impedance data according to a graphical representation method, which does not involve any fitting (44). In brief, α was determined by plotting the imaginary part of the impedance as a function of frequency in logarithmic coordinates (Fig. 2 *A*). α was consistently calculated in the high-frequency region, significantly larger than the characteristic relaxation frequency, from the slope of the decaying region from 6 data points. For the particular data set in Fig. 2 *A*, the slope was fitted to the data points corresponding to the filled markers. Once α was obtained, Q_{eff} was determined from the imaginary part of the impedance, Z_{im}, according to Eq. 2:

$$Q_{eff} = \sin\left(\frac{\alpha\pi}{2}\right)\frac{-1}{Z_{im}(f)(2\pi f)^{\alpha}} \quad (2)$$

Fig. 2 *B* shows calculated values of Q_{eff}, according to Eq. 2, as a function of frequency in logarithmic coordinates. An average over the values for the 6 data points of the high-frequency asymptote, corresponding to the frequencies used to calculate α, was used to determine Q_{eff}. Finally, the effective capacitance, C_{eff}, of the skin membrane was calculated by Eq. 3 from the average value of Q_{eff} and the corresponding values of α and R_{mem}.

$$C_{eff} = Q_{eff}^{1/\alpha} R_{mem}^{(1-\alpha)/\alpha} \quad (3)$$

The values of R_{mem}, α, Q_{eff}, and C_{eff}, corresponding to the impedance data in Fig. 2, are compiled in Table S3.

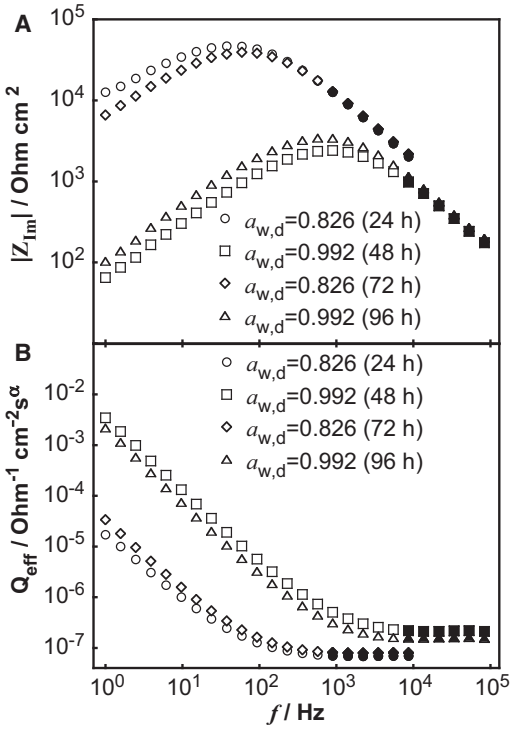

FIGURE 2 Skin membrane impedance data in logarithmic coordinates after 24 h, 48 h, 72 h, and 96 h with varying water activities in the donor solution ($a_{w,d}$). (*A*) Imaginary part of the impedance as a function of frequency. (*B*) Effective CPE parameter, Q_{eff}, as a function of frequency. Solid symbols represent data points used to determine CPE parameters α and Q_{eff}.

RESULTS

The aim of this study was to investigate the influence of hydration on the electrical properties of excised skin membranes. Solid-state NMR and x-ray diffraction measurements on SC samples were performed to allow for a molecular interpretation of the changes in the skin membrane impedance properties. The validity of using excised skin membranes for impedance measurements and SC samples in the NMR and x-ray experiments is discussed in the Supporting Material, Text C.

Impedance measurements on skin membranes under the influence of a varying water gradient

Skin membranes were placed in the Franz cell separating two bulk solutions. The water gradient across the skin membrane was controlled by the water activities in the surrounding solutions. The water activity on the SC side of the skin membrane (donor solution) was changed every 24 h between $a_{w,d} = 0.826$ and $a_{w,d} = 0.992$, and the water activity on the dermis side (receptor solution) was kept constant at $a_{w,r} = 0.992$.

The water gradient has a pronounced effect on skin membrane resistance (R_{mem})

The effect of a varying water gradient on the skin membrane resistance, R_{mem}, is demonstrated in Fig. 3, *A* and *B*, for two identical experiments using two different skin membranes. The results illustrate the natural variability of R_{mem} generally observed for different skin membranes (7, 20, 23, 27, 28). Of more importance, the changes of R_{mem} follow the same qualitative trends under the influence of a varying water gradient. The experiments start with the lower level of water activity in the donor solution (i.e., $a_{w,d} = 0.826$). At first, R_{mem} increases from time zero to a plateau value that is reached after a few hours. After 24 h, $a_{w,d}$ is changed from 0.826 to 0.992 (i.e., from PEG to PBS solution) and R_{mem} immediately drops down to a substantially lower value. The lower plateau value is maintained until 48 h, when the donor solution is again changed and the cycle is then repeated. Mean values of R_{mem}, corresponding to the data points collected over the last 2 h of each time period, are compiled in Table 1. On average, R_{mem} was ~ 14 times higher when $a_{w,d} = 0.826$ than when $a_{w,d} = 0.992$.

The water gradient affects membrane capacitance (C_{eff})

The effective membrane capacitance (C_{eff}) was determined from impedance data from each 24 h period. The results from two different skin membranes are shown as plots of C_{eff} over time (Fig. 4, *A* and *B*) and as average values of the data points collected over the last hours of each time

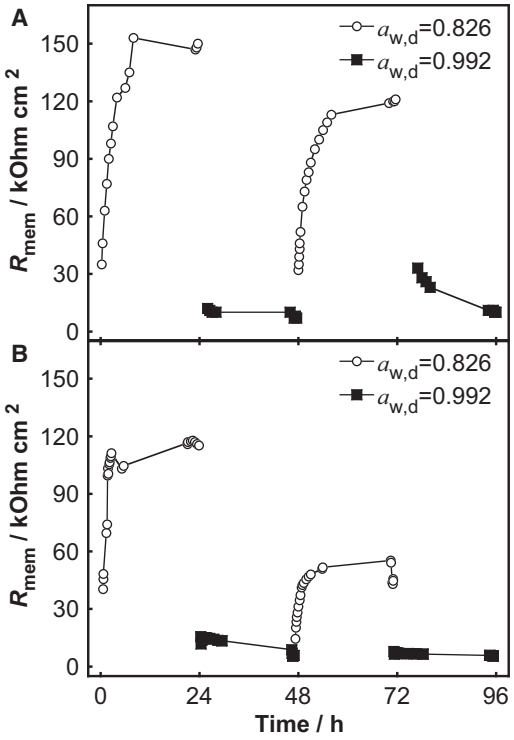

FIGURE 3 R_{mem} as a function of time for two skin membranes (*A* and *B*) with water gradient as a varying parameter. The water gradient was varied every 24 h by changing the water activity in the donor solution ($a_{w,d}$) on top of the skin membrane. The water activity of the receptor solution was constant at $a_{w,r} = 0.992$.

period (Table 1). The plots in Fig. 4 display a general pattern with lower values of C_{eff} when the $a_{w,d} = 0.826$ compared to when $a_{w,d} = 0.992$. On average, C_{eff} was ~ 1.5 times higher when $a_{w,d} = 0.992$ than when $a_{w,d} = 0.826$.

The effect of hydration on the molecular mobility of SC components as observed by PT ssNMR

To relate the impedance data to the molecular dynamics of the SC components, we performed PT ssNMR experiments on SC equilibrated in solutions with either $a_w = 0.826$ or $a_w = 0.992$. The complex mixture of molecular species in the SC is reflected in the multitude of ^{13}C resonances observed in Fig. 5, which shows overlaid DP (gray), CP (blue), and INEPT (red) spectra of SC samples. We have recently performed a complete assignment of most resonance lines and identified relevant markers for the protein and lipid components for intact SC (45). The Gly C_α (43.7 ppm), Ser C_α (56.7 ppm), and Ser C_β (62.4 ppm) peaks are suitable for probing the terminal domains of the keratin filaments due to their high abundance in the N- and C-terminal domains of the keratin filaments. Leu C_β and Lys C_ε (both at 40.6 ppm) can be used to probe the keratin filament coiled-coil core, as these residues are highly enriched in this domain. The lipid carbons represent a minor fraction of the total number of carbons in SC. However, most of the lipid species contain very long saturated hydrocarbon chains in the range C14–C32 (46,47), of which the majority of carbons give rise to peaks at similar chemical shifts. The methylene groups with all-*trans* conformations resonate at 33.4 ppm, and methylene groups exhibiting a distribution of *trans*/gauche conformations resonate at 30.5 ppm (48). In addition to the main methylene carbon peaks, the terminal carbons of the lipid chains, ωCH_3 (14.6 ppm) and (ω-1) CH_2 (23.3 ppm), are good markers for the lipid matrix. These signature peaks, for keratin filaments and lipids, are labeled in Fig. 5 *B*.

From Fig. 5, qualitative information on the molecular mobility is obtained by comparing the signal enhancement efficiency of INEPT (red) and CP (blue) with respect to the DP (gray). First, we conclude that the SC samples equilibrated at $a_w = 0.826$ (Fig. 5 *A*) or $a_w = 0.992$ (Fig. 5 *B*) display almost identical spectra compared to the SC samples equilibrated at 80% RH or 99.5% RH in Fig. S4, *A* and *B*. This is an important observation and proves that the experimental method used to regulate the water activity (i.e., adding a polymer to the donor solution) is sound. This observation also implies that the different type of medium used for equilibration (i.e., buffered solution or nonbuffered vapor phase), which in principle could lead to different effects related to the pH (49), does not seem to influence the molecular dynamics. In other words, it is reasonable to assume that the observed effects on the skin membrane impedance properties are governed by the degree of hydration, determined by the gradient in water activity across the skin membrane.

In general, the majority of the SC components are rigid (high anisotropy and/or in the slow regime), as indicated by the dominating CP signal for most of the spectral range under both experimental conditions. A clear effect of the

TABLE 1 Average values of R_{mem} and C_{eff}

		Membrane A		Membrane B	
Donor formulation	$a_{w,d}$	R_{mem} (kOhm cm^2)	C_{eff} (nF cm^{-2})	R_{mem}	C_{eff}
PEG (22–24 h)	0.826	148.2 ± 1.2	22.9 ± 0.7	116.4 ± 1.0	22.9 ± 1.0
PBS (46–48 h)	0.992	7.4 ± 0.1	31.1 ± 0.3	6.6 ± 1.5	40.4 ± 0.9
PEG (70–72 h)	0.826	119.9 ± 1.0	23.2 ± 0.1	47.3 ± 5.3	26.5 ± 0.5
PBS (94–96 h)	0.992	10.6 ± 0.2	26.9 ± 0.6	5.7 ± 0.2	40.1 ± 0.7

Values are given as the mean ± SD of $n = 3$–8 data points.

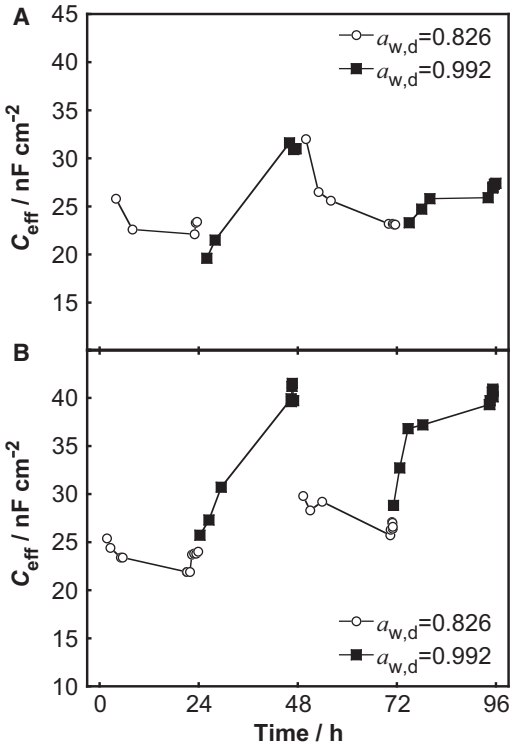

FIGURE 4 C_{eff} as a function of time for two skin membranes (*A* and *B*) with water gradient as a varying parameter. The water gradient was varied each 24 h by changing the water activity in the donor solution ($a_{w,d}$) on top of the skin membrane. The water activity of the receptor solution was constant at $a_{w,r} = 0.992$.

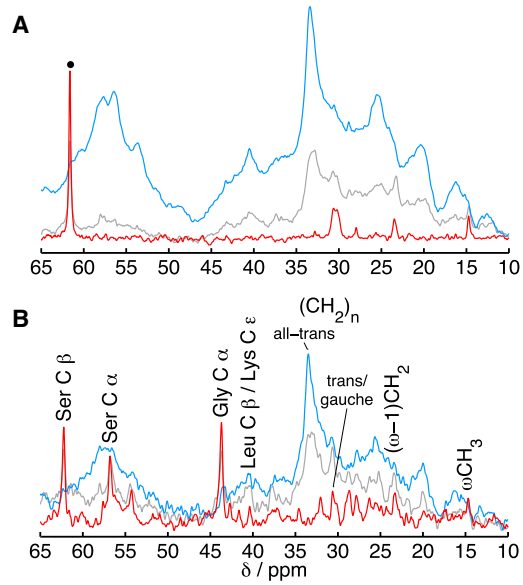

FIGURE 5 Molecular dynamics of SC components using DP (gray), CP (blue), and INEPT (red) pulse sequences for signal enhancement of molecular segments in either rigid (CP) or mobile (INEPT) microenvironments. ^{13}C spectra of SC equilibrated in solutions with $a_w = 0.826$ (the peak marked with a dot is from PEG) (*A*) and $a_w = 0.992$ (*B*). Resonance lines from SC lipids and amino acid residues of the SC proteins are labeled in *B*. The intensity is scaled to give an equal DP signal of the peak centered around 32.8 ppm due to the different amounts of SC sample in each experiment.

water activity on the dynamics of the terminal domains of the keratin filaments is observed. The INEPT signal from the peaks corresponding to Gly C_α, Ser C_α, and Ser C_β resonances is completely absent in the spectrum in Fig. 5 *A* ($a_w = 0.826$), whereas these peaks are significantly enhanced in the spectrum in Fig. 5 *B* ($a_w = 0.992$). This proves that the terminal domains of the keratin filaments are immobilized at $a_w = 0.826$ (i.e., the slow regime and/or high anisotropy in Fig. 1), whereas they are highly mobile at $a_w = 0.992$ (i.e., low anisotropy in the fast regime in Fig. 1). INEPT and CP peaks with identical line shapes and comparable amplitudes are generally observed for anisotropic liquid crystalline phases (24,31). However, none of the Gly C_α, Ser C_α, or Ser C_β INEPT resonances are accompanied by a CP peak, suggesting that these molecular segments are in a nearly isotropic microenvironment at $a_w = 0.992$. The CP signal enhancement from the Leu C_β and Lys C_ε resonances (40.5 ppm) is more pronounced in the spectrum of Fig. 5 *A* ($a_w = 0.826$), as compared to the spectrum in Fig. 5 *B* ($a_w = 0.992$). This implies that the mobility of residues in the coiled-coil core of the keratin filaments is increased by hydration, thus rendering the CP enhancement less efficient.

Turning to the lipid lamellae, it is seen that the enhancement of the CP signal from the all-*trans* $(CH_2)_n$ peak at 33.4 ppm is prominent in both spectra, showing that the majority of the methylene chain carbons remain in a rigid all-*trans* configuration. Three minor INEPT peaks are present in Fig. 5 *A* ($a_w = 0.826$), corresponding to the *trans*/gauche $(CH_2)_n$, $(\omega\text{-}1)CH_2$, and ωCH_3 resonances, proving that a minor fraction of the lipids are mobile even in the less hydrated SC membrane. The enhancement efficiency of the INEPT signal from these molecular segments is similar in Fig. 5 *B* ($a_w = 0.992$).

A final remark is that the enhancement efficiency of the CP signal over the complete spectral range is weaker from the sample equilibrated at $a_w = 0.992$ (Fig. 5 *B*) compared to the sample equilibrated at $a_w = 0.826$ (Fig. 5 *A*), suggesting that the molecular dynamics is, in general, characterized by faster reorientation and/or lower anisotropy at $a_w = 0.992$. This is in agreement with proton NMR studies on the SC, showing a gradual increase in the mobile components of the SC upon hydration (50,51). It is noteworthy that the relative intensity ratio of the CP and DP signals from the main methylene peak at 33.4 ppm is lower at $a_w = 0.992$, implying that the rigidity of the lipids decreases upon hydration.

The effect of hydration on the lipid lamellae and protein components of the SC as observed by SAXD and WAXD

SAXD and WAXD measurements were performed in a manner similar to that used for NMR measurements to

investigate the molecular organization of the lipid lamellae and the soft keratin components. We start by concluding that the diffraction curves of the SC samples equilibrated at $a_w = 0.826$ or at $a_w = 0.992$ (Fig. 6, *A* and *B*) are similar compared to the corresponding diffraction curves of the SC samples equilibrated in vapor with 80% RH or 99.5% RH (see Fig. S5, *A* and *B*).

In general, the peaks in Fig. 6 *A* from the SAXD measurements are broad and weak. The low Q range is dominated by strong scattering mainly attributed to protein structures of the SC (52,53). The diffraction curve from the SC sample equilibrated at $a_w = 0.992$ (Fig. 6 *A*, *upper curve*) shows diffraction peaks/shoulders centered around $Q = 0.5$ nm^{-1} (12.6 nm in d-spacing), $Q = 1.0$ nm^{-1} (6.3 nm in d-spacing), $Q = 1.4$ nm^{-1} (4.5 nm in d-spacing), and $Q = 1.8$ nm^{-1} (3.4 nm in d-spacing). This is in agreement with previous diffraction studies on pig SC (53) and suggests that the lipids are organized according to at least one lamellar phase with repeat distances of ~ 12.6 nm. The diffraction curve corresponding to the SC sample equilibrated at $a_w = 0.826$ is similar. However, the peak around $Q = 1.4$ nm^{-1} is slightly shifted to a smaller d-spacing of 4.3 nm and the diffraction peaks are in general weaker. One exception to this is the peak at $Q = 1.8$ nm^{-1}, which is more prominent. This peak indicates phase-separated crystalline cholesterol, which has been observed in intact pig SC (53), occasionally in human SC (54,55), but not typically in mouse SC (56–58). Studies on extracted SC ceramides, palmitic acid, and cholesterol have shown that the appearance of phase-separated cholesterol is sensitive to both lipid composition and hydration state (59,60). Taken together, the variation in intensity of the peak at $Q = 1.8$ nm^{-1} in Fig. 6 *A* may be related to an altered fraction of phase-separated crystalline cholesterol due to the difference in hydration state. However, we note that the SC sample at $a_w = 0.992$ (Fig. 6 *A*) has a weak peak at $Q = 1.8$ nm^{-1}, whereas the corresponding SC sample at RH = 99.5% does not (Fig. S5 *A*). This implies that phase-separated cholesterol may also be dependent on SC variability or how the sample was prepared. Even though it is beyond the scope of this study, we performed an experiment showing that the sample history can influence the appearance of crystalline cholesterol, as shown in Fig. S6.

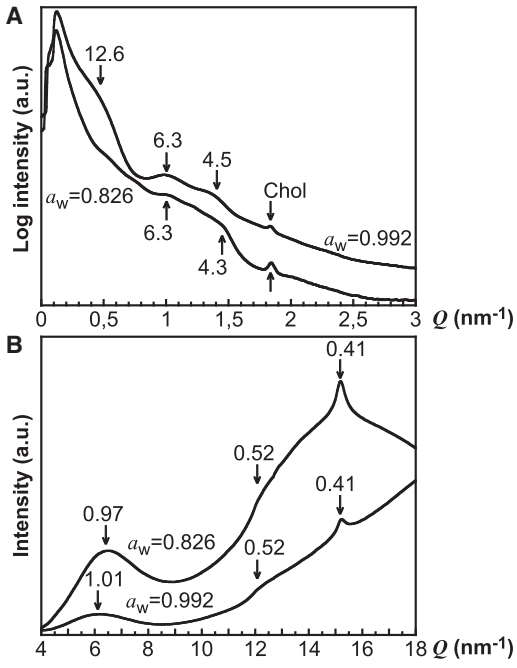

FIGURE 6 SAXS (*A*) and WAXS (*B*) data on SC at $a_w = 0.826$ and $a_w = 0.992$. Numbers associated with an arrow give the d-spacing (nm). Chol is crystalline cholesterol.

The WAXD results in Fig. 6 *B* show a clear peak around $Q = 15.2$ nm^{-1} (0.41 nm in d-spacing) corresponding to a hexagonal packing of the lipid hydrocarbon chains, which is in agreement with previous studies on pig SC (53). The broad diffraction peak with a maximum around $Q = 6.2$–6.5 nm^{-1} is attributed to the interchain packing of the soft keratin structures (61,62). The d-spacing of this peak is ~ 0.97 nm at $a_w = 0.826$ and ~ 1.01 nm at $a_w = 0.992$, which suggests that the soft keratin structures are more densely packed in the less hydrated SC sample as compared to packing in the fully hydrated SC sample. Considering that the preparation of the SC samples involves full hydration, complete dehydration, and final hydration at either $a_w = 0.826$ or $a_w = 0.992$, it is likely that the change in interchain d-spacing is reversible and determined by the SC hydration state (61,62). In general, the diffraction from amorphous keratin is poor. However, a very weak shoulder is observed at Q ~ 12 nm^{-1} (0.52 nm in d-spacing), which may indicate that a minor portion of the SC proteins have α-helical secondary structure (63).

DISCUSSION

The water gradient affects the skin membrane resistance (R_{mem}) in a reversible manner

The parameter R_{mem} reflects the resistance of ion transport encountered inside the skin membrane at frequencies approaching zero. The results show that the water gradient has a clear and reversible effect on R_{mem} (Fig. 3). On average, R_{mem} is 14 times lower when the water gradient is zero ($a_{w,r} = a_{w,d} = 0.992$). It should be noted that R_{mem} in general is gradually decreased over time, but the qualitative trends remain unaffected. To explain the changes in R_{mem}, it is appropriate to start by considering where the ions are distributed in the SC and how this distribution is affected by the varying water gradient. Several investigators have suggested that ions are primarily transported and hence distributed in the extracellular domains (64,65). It has also been shown that prolonged hydration times (as in this study) can lead to both intracellular and extracellular accumulation

of ions (65). The dramatic change in R_{mem} implies that changes of the molecular organization and/or changes of the molecular dynamics of the SC components occur. If the ions are primarily distributed in the continuous extracellular lipid regions, the data imply that hydration influences the properties of theses domains. If the ions are also distributed in the intracellular domains, then the effect of hydration on the protein structures also needs to be considered. To distinguish between these possibilities, the data on membrane resistance are evaluated together with the characterization of the molecular structure and the dynamics of the SC components.

The NMR data show that the majority of the methylene carbons in the SC lipid chains are in a rigid all-*trans* configuration at both water activities investigated, and that only a minor fraction of the lipids are fluid (Fig. 5). Furthermore, for both water activities, the diffraction data show lipid lamellar structures with similar repeat distances (Fig. 6 *A*) and a hexagonal packing of the lipid hydrocarbon chains (Fig. 6 *B*). The combination of the results in Fig. 5 and Fig. 6 suggests that the organization of the lipid lamellae is similar at both hydration conditions. However, an increased fraction of mobile lipids upon hydration has been observed in infrared, electron spin resonance, and proton NMR studies of the SC (21,66,67), suggesting that the dynamics of the SC lipids is affected by hydration. We have recently explored the effect of hydration of the SC and observed a gradual increase in the enhancement efficiency of the INEPT lipid signature peaks between 0% RH and 90% RH, whereas hydration above 90% RH resulted in a slight decrease in INEPT enhancement efficiency of these peaks (45). The proposed explanation is that the dynamics of the mobile SC lipids first increase and then gradually slow down due to changes in the chemical composition of the fluid lipid phase. Between 0% RH and 90% RH, short-chain and more polar lipids are fluid, and above 90% RH, the fluid fraction contains long-chain lipids and cholesterol. In support of this interpretation, we note that the intensity of the diffraction peak from crystalline cholesterol decreased upon hydration (Fig. 6 *A*). This effect is most clear in Fig. S5 *A*, where the cholesterol peak is present in the diffraction curve for the SC equilibrated at 80% RH, but completely absent at 99.5% RH. This implies that the fraction of phase-separated crystalline cholesterol is reduced by being incorporated into the lamellar structures upon hydration. This is in line with the observed phase separation of cholesterol in a dehydrated lipid mixture of extracted SC ceramides, palmitic acid, and cholesterol, as compared to the same mixture in the hydrated state, where no phase separation was observed (59). As cholesterol and long-chain lipids have a slower reorientation rate, they will slow down the rate of the smaller molecules by increasing the viscosity of the fluid lipid phase, which decreases the INEPT signal from the fluid lipid signature peaks. Fig. 5 also shows that the CP over DP signal intensity ratio of the main methylene peak is lower at higher hydration, showing less lipid rigidity. Considering these data together, we suggest that the majority of the lipids remain in a rigid lamellar structure with all-*trans* configuration, whereas a minor fraction of fluid lipids is present that increases upon hydration. It is possible that the mobilization of lipids may accommodate stress caused by swelling of corneocytes. The spatial distribution of the fluid lipid domains cannot, however, be determined from the PT ssNMR results and thus remains unclear. Considering the drastic decrease in R_{mem}, we suggest that microdomains of fluid lipids can contribute to conductive regions, which then increase in size and/or become more interconnected in the fully hydrated SC, leading to the observed decrease in R_{mem}.

If the ions are also distributed in the intracellular domains (65), we need to consider the effect of hydration on the corneocytes. When the SC membrane is less hydrated ($a_{w,d} = 0.826$), the amino acid residues of the keratin filaments are highly rigid, as seen from the dominant enhancement of the CP signal and the absence of INEPT signal (Fig. 5 *A*). Further, the interchain packing of the keratin filaments is more dense (Fig. 6 *B*). A likely consequence of these observations is that any intracellular ions will be more restricted in the less hydrated state. When the SC is fully hydrated ($a_{w,d} = 0.992$), the keratin filaments are more mobile, as observed from the prominent enhancement of the INEPT signal from the glycine and serine resonances and the relatively weaker enhancement of the CP signal (Fig. 5 *B*). The packing of the keratin filaments is slightly expanded with a larger interchain spacing (Fig. 6 *B*), which can be related to a nearly isotropic reorientation of the terminal domains (Fig. 5 *B*). These results imply that the conductive domains in the intracellular regions are increased in size and may have a higher concentration of mobile ions in the hydrated state. However, this alone cannot explain the observed decrease in R_{mem}, as the reduction of zero-frequency resistance in all cases will depend on the restriction of ion transport across the whole SC, which includes both the isolated corneocytes and the continuous extracellular lipid lamellar structures. In respect to this, it may be relevant to consider the presence of corneodesmosomes, which potentially can represent an interconnected passage acting to decrease R_{mem}, especially in the deeper regions of the SC where they are more abundant (68).

We note, finally, that R_{mem} can be affected by the solution resistance (7,8), which in this work varied between R_{sol} ~ 1500 Ohm (65 wt % PEG in PBS solution) and R_{sol} ~ 200 Ohm (neat PBS solution). To investigate this further, we performed two control experiments. In conclusion, the results show that the mechanisms responsible for the changes in R_{mem}, as a consequence of a varying water gradient, cannot simply be explained by the variations of R_{sol} (see the Supporting Material, Text D).

The water gradient affects the membrane effective capacitance (C_{eff}) in a reversible manner

The capacitance of the skin membrane has been attributed mainly to the dielectric nature of lipid structures that impede transport of ions in the SC membrane (8,16,18,19). In support of this, it has been shown that elevated temperatures affect the skin membrane capacitance; it remains fairly constant below 30°C and increases abruptly at temperatures >~ 60°C (8,18,69). The abrupt increase in skin capacitance above 60°C correlates with the generally observed major thermal event occurring around this temperature in DSC measurements of the SC (66,70), which has been shown to be associated with a phase transition occurring in the extracellular lipid domains (71). However, to our knowledge, it has never been shown that a varying water gradient can induce a similar but less pronounced effect on the skin membrane capacitance. The results in this work show that on average, C_{eff} is 1.5 times higher in the case of a fully hydrated skin membrane (Fig. 4).

If the C_{eff} is attributed solely to the lipid domains in the skin membrane, then these domains can be visualized as a dielectric medium between the corneocytes. In this case, the capacitance (F cm^{-2}) depends on the thickness, d, and the dielectric constant, ε, of these domains, according to

$$C_{eff} = \frac{\varepsilon_0 \varepsilon}{d}, \quad (4)$$

where ε_0 is the permittivity of vacuum (8.9×10^{-14} F cm^{-1}). As shown in this study (Fig. 6 *A*), which confirms results of previous studies (53,61), the swelling of the lipid lamellar structures is minor upon hydration. Thus, it is reasonable to assume that d is not affected by hydration. For dry skin, the corneocyte thickness is ~ 0.8 μm and the thickness of the lipid domain between two corneocytes is ~ 0.075 μm (72,73). The thickness of the SC is ~ 15 μm (74,75), which means that the total thickness (d) of the lipid domains should be ~ 1.3 μm, assuming that the corneocytes and lipid domains are stacked upon each other in a repeating manner. C_{eff} was on average 24 nF cm^{-2} when $a_{w,d} = 0.826$ and 35 nF cm^{-2} when $a_{w,d} = 0.992$. Then, it follows from Eq. 4 that the dielectric constant of the capacitive domains is ε ~ 35 when $a_{w,d} = 0.826$ and ε ~ 51 when $a_{w,d} = 0.992$. This estimate gives values in agreement with those previously suggested for the dielectric constant of SC: ε ~ 10 for dry SC (76) and ε ~ 49 for hydrated SC in contact with a buffered electrolyte solution (conditions similar to those applied here) (41). Even if the calculated values of ε are only rough estimates from a simplified model, they indicate that hydration affects the dielectric properties of the SC components. As discussed above, we suggest that the fraction of fluid lipids increases upon hydration, which implies that the dielectric constant increases in these domains upon incorporation of water molecules. In addition, the fatty acids in the SC lipids can be affected by hydration in that the dissociation equilibrium changes. It is therefore possible that the local proton concentration in the lipid lamellar structures is affected by the degree of hydration (49). This may result in a higher charge density in the headgroup regions of the lipid lamellae in the case of the fully hydrated skin membrane, which could increase C_{eff} by providing more charged sites for double-layer capacitance. We note that increased charge density of fatty acids at elevated pH has been shown for lipid lamellar structures containing extracted SC ceramides, palmitic acid, and cholesterol (77). However, as the solutions in contact with the skin membrane in this work are buffered, it is unclear whether this effect is relevant here.

The estimated values of ε (~ 35–51) are in strong contrast to the dielectric constant of lipids, which is in the range ε ~ 2–4. On the other hand, if ε is assumed to be 3, then the average thickness of the capacitive domains is ~ 0.11 μm when $a_{w,d} = 0.826$ and 0.08 μm when $a_{w,d} = 0.992$ (calculated with the average values of C_{eff}). This line of reasoning indicates that the capacitive domains in the SC are either considerably smaller than the expected total lipid lamellar thickness or that the dielectric constant is considerably larger than for a hydrocarbon bilayer. The latter implies that components of the SC other than the lipid lamellae contribute to the capacitive currents. For example, a double-layer capacitance may be due to charged species of the SC, which are balanced by electrolyte ions, as previously suggested (40). This mechanism might be of particular relevance in the case of a fully hydrated SC membrane, considering that the interchain packing of the keratin filaments is expanded (Fig. 6 *B*) and that the terminal domains undergo nearly isotropic reorientation at $a_{w,d} = 0.992$ (Fig. 5 *B*). In other words, any charged amino acid residues present in the mobile terminal domains are more freely accessible for double-layer charging in the fully hydrated SC membrane and may contribute to the observed increase in C_{eff} at increased SC hydration.

The relation between skin impedance and permeability

Previous investigations have demonstrated an inverse linear relationship between passive diffusion (permeability coefficient) of highly hydrophilic molecules (e.g., water (16), urea (78), mannitol (79,80), inulin (80), and sodium ions (81)) and membrane resistance in logarithmic coordinates. This correlation is only moderate for hydrophobic molecules, such as corticosterone and estradiol (80). In a similar manner, there is a relationship between the changes of the skin membrane electrical properties observed in this study and the steady-state flux of model drugs under the influence of a varying water gradient (2). When the skin membrane is more hydrated, it has a lower membrane resistance, higher effective capacitance, and higher drug permeability. The opposite is true for a less hydrated membrane. This shows

that impedance measurements provide important and complementary information on how skin permeability is affected by external parameters such as the water gradient, which may prove to be useful in future investigations.

CONCLUSIONS

We have investigated the effect of a varying water gradient on the electrical properties of skin membranes. We performed ^{13}C PT ssNMR and x-ray diffraction measurements on SC samples to obtain information regarding their molecular structure and dynamics under similar hydration conditions. The main conclusions are as follows.

1. The SC lipids are organized into lamellar structures with ~ 12.6-nm spacing and hexagonal hydrocarbon chain packing with a mainly all-*trans* configuration of the acyl chains, irrespective of hydration state. A fraction of fluid lipids is present and is suggested to increase upon hydration due to mobilization and incorporation of cholesterol and long-chain lipids.
2. Keratin filaments are rigid structures with closer interchain spacing in the dehydrated state. Hydration increases the dynamics of the keratin filament terminal domains and the interchain spacing.
3. Impedance measurements show that R_{mem} and C_{eff} are affected by hydration due to changes in the water gradient and that the effect is largely reversible.
4. The strong decrease of R_{mem} indicates that ion transfer inside the SC becomes less restricted upon hydration. Increased ion transfer can be related to hydration-induced lipid mobility in the extracellular continuous lamellae.
5. The changes in mobility of the intracellular protein components upon hydration/dehydration may influence the mobility of intracellular ions. However, the effect of this on R_{mem} is in all cases dependent on the ability of ions to cross the extracellular lipids (see conclusion 4).
6. The observed increase in C_{eff} indicates that the dielectric properties of the capacitive domains are affected by hydration. We attribute this effect to hydration-induced lipid fluidity and/or contributions to double-layer capacitance from a larger fraction of accessible and charged amino acid residues of the keratin filament terminals upon hydration.

SUPPORTING MATERIAL

Supporting methods, seven figures, and four tables are available at http://www.biophysj.org/biophysj/supplemental/S0006-3495(13)00533-X.

We thank Krister Thuresson for valuable discussions, and Tomás Plivelic, Sylvio, Haas, Dörthe Haase, and Yngve Cerenius for assistance at MaxLab (Lund, Sweden).

We thank the Research School in Pharmaceutical Sciences (S.B., E.S., and J.E.), the Knowledge Foundation (J.E. and T.R.), the Gustaf Th Ohlssons Foundation (J.E. and T.R.), the Swedish Foundation for Strategic Research (E.S.), and the Swedish Research Council (E.S. and D.T.) for financial support.

REFERENCES

1. Scheuplein, R. J., and I. H. Blank. 1971. Permeability of the skin. *Physiol. Rev.* 51:702–747.
2. Björklund, S., J. Engblom, …, E. Sparr. 2010. A water gradient can be used to regulate drug transport across skin. *J. Control. Release.* 143:191–200.
3. Zhai, H., and H. Maibach. 2001. Effects of skin occlusion on percutaneous absorption: an overview. *Skin Pharmacol. Appl. Skin Physiol.* 14:1–10.
4. Karande, P., A. Jain, …, S. Mitragotri. 2005. Design principles of chemical penetration enhancers for transdermal drug delivery. *Proc. Natl. Acad. Sci. USA.* 102:4688–4693.
5. Prausnitz, M. R., V. G. Bose, …, J. C. Weaver. 1993. Electroporation of mammalian skin: a mechanism to enhance transdermal drug delivery. *Proc. Natl. Acad. Sci. USA.* 90:10504–10508.
6. Pliquett, U., R. Langer, and J. C. Weaver. 1995. Changes in the passive electrical properties of human stratum corneum due to electroporation. *Biochim. Biophys. Acta.* 1239:111–121.
7. DeNuzzio, J. D., and B. Berner. 1990. Electrochemical and iontophoretic studies of human skin. *J. Control. Release.* 11:105–112.
8. Oh, S. Y., L. Leung, …, R. O. Potts. 1993. Effect of current, ionic strength and temperature on the electrical properties of skin. *J. Control. Release.* 27:115–125.
9. Blichmann, C. W., and J. Serup. 1988. Assessment of skin moisture. Measurement of electrical conductance, capacitance and transepidermal water loss. *Acta Derm. Venereol.* 68:284–290.
10. Madison, K. C., D. C. Swartzendruber, …, D. T. Downing. 1987. Presence of intact intercellular lipid lamellae in the upper layers of the stratum corneum. *J. Invest. Dermatol.* 88:714–718.
11. Weerheim, A., and M. Ponec. 2001. Determination of stratum corneum lipid profile by tape stripping in combination with high-performance thin-layer chromatography. *Arch. Dermatol. Res.* 293:191–199.
12. Candi, E., R. Schmidt, and G. Melino. 2005. The cornified envelope: a model of cell death in the skin. *Nat. Rev. Mol. Cell Biol.* 6:328–340.
13. Steinert, P. M., and L. N. Marekov. 1995. The proteins elafin, filaggrin, keratin intermediate filaments, loricrin, and small proline-rich proteins 1 and 2 are isodipeptide cross-linked components of the human epidermal cornified cell envelope. *J. Biol. Chem.* 270:17702–17711.
14. Swartzendruber, D. C., P. W. Wertz, …, D. T. Downing. 1987. Evidence that the corneocyte has a chemically bound lipid envelope. *J. Invest. Dermatol.* 88:709–713.
15. Yamamoto, T., and Y. Yamamoto. 1976. Electrical properties of the epidermal stratum corneum. *Med. Biol. Eng.* 14:151–158.
16. Kalia, Y. N., F. Pirot, and R. H. Guy. 1996. Homogeneous transport in a heterogeneous membrane: water diffusion across human stratum corneum in vivo. *Biophys. J.* 71:2692–2700.
17. Clar, E. J., C. P. Her, and C. G. Sturelle. 1975. Skin impedance and moisturization. *J. Soc. Cosmet. Chem.* 26:337–353.
18. Craane-van Hinsberg, W. H. M., J. C. Verhoef, …, H. E. Bodde. 1995. Thermoelectrical analysis of the human skin barrier. *Thermochim. Acta.* 248:303–318.
19. Kalia, Y. N., and R. H. Guy. 1995. The electrical characteristics of human skin in vivo. *Pharm. Res.* 12:1605–1613.
20. Foley, D., J. Corish, and O. I. Corrigan. 1992. Iontophoretic delivery of drugs through membranes including human stratum corneum. *Solid State Ion.* 53–56:184–196.
21. Alonso, A., N. C. Meirelles, …, M. Tabak. 1996. Water increases the fluidity of intercellular membranes of stratum corneum: correlation

with water permeability, elastic, and electrical resistance properties. *J. Invest. Dermatol.* 106:1058–1063.

22. Blank, I. H., J. Moloney, 3rd, …, C. Apt. 1984. The diffusion of water across the stratum corneum as a function of its water content. *J. Invest. Dermatol.* 82:188–194.
23. Campbell, S. D., K. K. Kraning, …, S. T. Momii. 1977. Hydration characteristics and electrical resistivity of stratum corneum using a noninvasive four-point microelectrode method. *J. Invest. Dermatol.* 69:290–295.
24. Nowacka, A., P. C. Mohr, …, D. Topgaard. 2010. Polarization transfer solid-state NMR for studying surfactant phase behavior. *Langmuir.* 26:16848–16856.
25. Björklund, S., J. Engblom, …, E. Sparr. 2013. Glycerol and urea can be used to increase skin permeability in reduced hydration conditions. *Eur. J. Pharm. Sci.* Epub ahead of print May 3, 2013.
26. Colin, E., W. Clarke, and D. Glew. 1985. Evaluation of the thermodynamic functions for aqueous sodium chloride from equilibrium and calorimetric measurements below 154°C. *J. Phys. Chem. Ref. Data.* 14: 489–610.
27. Rosell, J., J. Colominas, …, J. G. Webster. 1988. Skin impedance from 1 Hz to 1 MHz. *IEEE Trans Biomed Eng.* 35:649–651.
28. Tregear, R. T. 1965. Interpretation of Skin Impedance Measurements. *Nature.* 205:600–601.
29. Tsai, J. C., P. L. Hung, and H. M. Sheu. 2001. Molecular weight dependence of polyethylene glycol penetration across acetone-disrupted permeability barrier. *Arch. Dermatol. Res.* 293:302–307.
30. Tsai, J. C., L. C. Shen, …, C. C. Lu. 2003. Tape stripping and sodium dodecyl sulfate treatment increase the molecular weight cutoff of polyethylene glycol penetration across murine skin. *Arch. Dermatol. Res.* 295:169–174.
31. Nowacka, A., N. A. Bongartz, …, D. Topgaard. 2013. Signal intensities in ^{1}H-^{13}C CP and INEPT MAS NMR of liquid crystals. *J. Magn. Reson.* 230:165–175.
32. Morris, G. A., and R. Freeman. 1979. Enhancement of nuclear magnetic resonance signals by polarization transfer. *J. Am. Chem. Soc.* 101:760–762.
33. Pines, A., J. S. Waugh, and M. G. Gibby. 1972. Proton enhanced nuclear induction spectroscopy. A method for high-resolution NMR of dilute spins in solids. *J. Chem. Phys.* 56:1776–1777.
34. Bennett, A. E., C. M. Rienstra, …, R. G. Griffin. 1995. Heteronuclear decoupling in rotating solids. *J. Chem. Phys.* 103:6951–6958.
35. Chen, L., Z. Weng, …, M. Garland. 2002. An efficient algorithm for automatic phase correction of NMR spectra based on entropy minimization. *J. Magn. Reson.* 158:164–168.
36. van Beek, J. D. 2007. matNMR: a flexible toolbox for processing, analyzing and visualizing magnetic resonance data in Matlab. *J. Magn. Reson.* 187:19–26.
37. Labrador, A., Y. Cerenius, …, T. Plivelic. 2012. The yellow SAXS mini-hutch at MAX IV laboratory. 11th Internatl. Conf. Synchrotron Radiat. Instrum., Lyon, France, July 9–13.
38. Cole, K. S. 1968. Membranes, Ions, and Impulses. University of California Press, Berkeley.
39. Pliquett, F., and U. Pliquett. 1996. Passive electrical properties of human stratum corneum in vitro depending on time after separation. *Biophys. Chem.* 58:205–210.
40. Kontturi, K., and L. Murtomäki. 1994. Impedance spectroscopy in human skin. A refined model. *Pharm. Res.* 11:1355–1357.
41. Hirschorn, B., M. E. Orazem, …, M. Musiani. 2010. Determination of effective capacitance and film thickness from constant-phase-element parameters. *Electrochim. Acta.* 55:6218–6227.
42. Lackermeier, A. H., E. T. McAdams, …, A. D. Woolfson. 1999. In vivo ac impedance spectroscopy of human skin. Theory and problems in monitoring of passive percutaneous drug delivery. *Ann. N. Y. Acad. Sci.* 873:197–213.
43. Membrino, M. A. 2002. Transdermal delivery of therapeutic compounds by iontophoresis. Ph.D. thesis. Chemical Engineering, University of Florida, Gainesville, FL.
44. Orazem, M. E., N. Pebere, and B. Tribollet. 2006. Enhanced graphical representation of electrochemical impedance data. *J. Electrochem. Soc.* 153:B129–B136.
45. Björklund, S., A. Nowacka, …, D. Topgaard. 2013. Characterization of stratum corneum molecular dynamics by natural-abundance ^{13}C solid-state NMR. *PLoS ONE.* 8:e61889.
46. Schaefer, H., and T. E. Redelmeier. 1996. Composition and structure of the stratum corneum. *In* Skin Barrier: Principles of Percutaneous Absorption.. Karger, Basel, Switzerland. 43–86.
47. Wertz, P. W., and D. T. Downing. 1983. Ceramides of pig epidermis: structure determination. *J. Lipid Res.* 24:759–765.
48. Earl, W. L., and D. L. VanderHart. 1979. Observations in solid polyethylenes by carbon-13 magnetic resonance with magic angle sample spinning. *Macromolecules.* 12:762–767.
49. Åberg, C., H. Wennerström, and E. Sparr. 2008. Transport processes in responding lipid membranes: a possible mechanism for the pH gradient in the stratum corneum. *Langmuir.* 24:8061–8070.
50. Laule, C., S. Tahir, …, A. L. MacKay. 2010. A proton NMR study on the hydration of normal versus psoriatic stratum corneum: linking distinguishable reservoirs to anatomical structures. *NMR Biomed.* 23:1181–1190.
51. Vavasour, I. M., N. Kitson, and A. MacKay. 1998. What's water got to do with it? A nuclear magnetic resonance study of molecular motion in pig stratum corneum. *J. Investig. Dermatol. Symp. Proc.* 3:101–104.
52. Garson, J. C., J. Doucet, …, G. Tsoucaris. 1991. Oriented structure in human stratum corneum revealed by x-ray diffraction. *J. Invest. Dermatol.* 96:43–49.
53. Bouwstra, J. A., G. S. Gooris, …, D. T. Downing. 1995. Lipid organization in pig stratum corneum. *J. Lipid Res.* 36:685–695.
54. Bouwstra, J. A., G. S. Gooris, …, W. Bras. 1991. Structural investigations of human stratum corneum by small-angle x-ray scattering. *J. Invest. Dermatol.* 97:1005–1012.
55. Bouwstra, J. A., G. S. Gooris, …, W. Bras. 1992. Structure of human stratum corneum as a function of temperature and hydration: a wide-angle x-ray diffraction study. *Int. J. Pharm.* 84:205–216.
56. White, S. H., D. Mirejovsky, and G. I. King. 1988. Structure of lamellar lipid domains and corneocyte envelopes of murine stratum corneum. An x-ray diffraction study. *Biochemistry.* 27:3725–3732.
57. Bouwstra, J. A., G. S. Gooris, …, W. Bras. 1994. The lipid and protein structure of mouse stratum corneum: a wide and small angle diffraction study. *Biochim. Biophys. Acta.* 1212:183–192.
58. Ohta, N., S. Ban, …, I. Hatta. 2003. Swelling of intercellular lipid lamellar structure with short repeat distance in hairless mouse stratum corneum as studied by x-ray diffraction. *Chem. Phys. Lipids.* 123:1–8.
59. McIntosh, T. J., M. E. Stewart, and D. T. Downing. 1996. X-ray diffraction analysis of isolated skin lipids: reconstitution of intercellular lipid domains. *Biochemistry.* 35:3649–3653.
60. Bouwstra, J. A., K. Cheng, …, M. Ponec. 1996. The role of ceramides 1 and 2 in the stratum corneum lipid organisation. *Biochim. Biophys. Acta.* 1300:177–186.
61. Nakazawa, H., N. Ohta, and I. Hatta. 2012. A possible regulation mechanism of water content in human stratum corneum via intercellular lipid matrix. *Chem. Phys. Lipids.* 165:238–243.
62. Hey, M. J., D. J. Taylor, and W. Derbyshire. 1978. Water sorption by human callus. *Biochim. Biophys. Acta.* 540:518–533.
63. Kreplak, L., J. Doucet, …, F. Briki. 2004. New aspects of the α-helix to β-sheet transition in stretched hard α-keratin fibers. *Biophys. J.* 87:640–647.
64. Potts, R. O., R. H. Guy, and M. L. Francoeur. 1992. Routes of ionic permeability through mammalian skin. *Solid State Ion.* 53–56:165–169.

65. Bodde, H. E., I. Van den Brink, …, F. H. N. De Haan. 1991. Visualization of in vitro percutaneous penetration of mercuric chloride; transport through intercellular space versus cellular uptake through desmosomes. *J. Control. Release.* 15:227–236.

66. Gay, C. L., R. H. Guy, …, M. L. Francoeur. 1994. Characterization of low-temperature (i.e., $< 65^{\circ}$C) lipid transitions in human stratum corneum. *J. Invest. Dermatol.* 103:233–239.

67. Silva, C., D. Topgaard, …, E. Sparr. 2007. Stratum corneum hydration: phase transformations and mobility in stratum corneum, extracted lipids and isolated corneocytes. *Biochim. Biophys. Acta.* 1768:2647–2659.

68. Chapman, S. J., and A. Walsh. 1990. Desmosomes, corneosomes and desquamation. An ultrastructural study of adult pig epidermis. *Arch. Dermatol. Res.* 282:304–310.

69. Nolan, L. M. A., J. Corish, and O. I. Corrigan. 1993. Electrical properties of human stratum corneum and transdermal drug transport. *J. Chem. Soc., Faraday Trans.* 89:2839–2845.

70. Golden, G. M., D. B. Guzek, …, R. O. Potts. 1986. Lipid thermotropic transitions in human stratum corneum. *J. Invest. Dermatol.* 86: 255–259.

71. Babita, K., V. Kumar, …, A. K. Tiwary. 2006. Thermotropic and spectroscopic behavior of skin: relationship with percutaneous permeation enhancement. *Curr. Drug Deliv.* 3:95–113.

72. Charalambopoulou, G. C., P. Karamertzanis, …, A. T. Papaioannou. 2000. A study on structural and diffusion properties of porcine stratum corneum based on very small angle neutron scattering data. *Pharm. Res.* 17:1085–1091.

73. Johnson, M. E., D. Blankschtein, and R. Langer. 1997. Evaluation of solute permeation through the stratum corneum: lateral bilayer diffusion as the primary transport mechanism. *J. Pharm. Sci.* 86:1162–1172.

74. Corcuff, P., C. Bertrand, and J. L. Leveque. 1993. Morphometry of human epidermis in vivo by real-time confocal microscopy. *Arch. Dermatol. Res.* 285:475–481.

75. Holbrook, K. A., and G. F. Odland. 1974. Regional differences in the thickness (cell layers) of the human stratum corneum: an ultrastructural analysis. *J. Invest. Dermatol.* 62:415–422.

76. Rosendal, T. 1945. Concluding studies on the conducting properties of human skin to alternating current. *Acta Physiol. Scand.* 9:39–49.

77. McIntosh, T. J. 2003. Organization of skin stratum corneum extracellular lamellae: diffraction evidence for asymmetric distribution of cholesterol. *Biophys. J.* 85:1675–1681.

78. Peck, K. D., A. H. Ghanem, and W. I. Higuchi. 1995. The effect of temperature upon the permeation of polar and ionic solutes through human epidermal membrane. *J. Pharm. Sci.* 84:975–982.

79. Sims, S. M., W. I. Higuchi, and V. Srinivasan. 1991. Skin alteration and convective solvent flow effects during iontophoresis: I. Neutral solute transport across human skin. *Int. J. Pharm.* 69:109–121.

80. Karande, P., A. Jain, and S. Mitragotri. 2006. Relationships between skin's electrical impedance and permeability in the presence of chemical enhancers. *J. Control. Release.* 110:307–313.

81. Kasting, G. B., and L. A. Bowman. 1990. DC electrical properties of frozen, excised human skin. *Pharm. Res.* 7:134–143.